Delft University of Technology

Techno-economic assessment and operational CO_2 emissions of High-Temperature Aquifer Thermal Energy Storage (HT-ATES) using demand-driven and subsurface-constrained dimensioning

Daniilidis, Alexandros; Mindel, Julian E.; De Oliveira Filho, Fleury; Guglielmetti, Luca

DOI
10.1016/j.energy.2022.123682

Publication date
2022

Document Version
Final published version

Published in
Energy

Citation (APA)
Daniilidis, A., Mindel, J. E., De Oliveira Filho, F., & Guglielmetti, L. (2022). Techno-economic assessment and operational CO_2 emissions of High-Temperature Aquifer Thermal Energy Storage (HT-ATES) using demand-driven and subsurface-constrained dimensioning. *Energy*, *249*, Article 123682. https://doi.org/10.1016/j.energy.2022.123682

Important note
To cite this publication, please use the final published version (if applicable).
Please check the document version above.

Copyright
Other than for strictly personal use, it is not permitted to download, forward or distribute the text or part of it, without the consent of the author(s) and/or copyright holder(s), unless the work is under an open content license such as Creative Commons.

Takedown policy
Please contact us and provide details if you believe this document breaches copyrights.
We will remove access to the work immediately and investigate your claim.

This work is downloaded from Delft University of Technology.
For technical reasons the number of authors shown on this cover page is limited to a maximum of 10.

Energy 249 (2022) 123682

Contents lists available at ScienceDirect

Energy

journal homepage: www.elsevier.com/locate/energy

Techno-economic assessment and operational CO_2 emissions of High-Temperature Aquifer Thermal Energy Storage (HT-ATES) using demand-driven and subsurface-constrained dimensioning

Alexandros Daniilidis [a, *], Julian E. Mindel [b], Fleury De Oliveira Filho [c], Luca Guglielmetti [a]

[a] University of Geneva, Geo-Energy Reservoir Geology and Sedimentary Basin Analysis Group, Rue des Maraichers 13, Geneve, 1205, Switzerland
[b] ETH Inst. of Geochemistry and Petrology, Clausiusstrasse 25, 8092, Zurich, Switzerland
[c] Energy Systems Group, Department F.-A. Forel for Environmental and Aquatic Sciences (DEFSE), Institute for Environmental Sciences (ISE), University of Geneva, Switzerland

ARTICLE INFO

Article history:
Received 28 September 2021
Received in revised form
14 January 2022
Accepted 7 March 2022
Available online 14 March 2022

ABSTRACT

High-Temperature – Aquifer Thermal Energy Storage (HT-ATES) can significantly increase Renewable Energy Sources (RES) capacity and storage temperature levels compared to traditional ATES, while improving efficiency. Combined assessment of subsurface performance and surface District Heating Networks (DHN) is key, but poses challenges for dimensioning, energy flow matching, and techno-economic performance of the joint system. We present a novel methodology for dimensioning and techno-economic assessment of an HT-ATES system combining subsurface, DHN, operational CO_2 emissions, and economics. Subsurface thermo-hydraulic simulations consider aquifer properties (thickness, permeability, porosity, depth, dip, artesian conditions and groundwater hydraulic gradient) and operational parameters (well pattern and cut-off temperature). Subject to subsurface constraints, aquifer permeability and thickness are major control variables. Transmissivity $\geq 2.5 \times 10^{-12}$ m^3 is required to keep the Levelised Cost Of Heat (LCOH) below 200 CHF/MWh and capacity $\geq$25 MW is needed for the HT-ATES system to compete with other large-scale DHN heat sources. Addition of Heat Pumps (HP) increases the LCOH, but also the nominal capacity of the system and yields higher cumulative avoided CO_2 emissions. The methodology presented exemplifies HT-ATES dimensioning and connection to DHN for planning purposes and opens-up the possibility for their fully-coupled assessment in site-specific assessments.

© 2022 The Authors. Published by Elsevier Ltd. This is an open access article under the CC BY-NC license (http://creativecommons.org/licenses/by-nc/4.0/).

1. Introduction

The heating and cooling sector covers a broad range of end-use applications and technologies such as water heating, ambient heating, ambient cooling and refrigeration in the building sector. In industry, it also includes process heating with operating temperature ranges from low temperature applications (e.g., in the food industry) to high temperature applications (e.g., in the cement, iron and steel industries) [1]. A study on the EU-28 countries, including Switzerland, Norway and Iceland reported that final energy demand for heating and cooling amounts to 51% of the energy use, of which 66% is fossil based [2]. Space Heating (SH) in EU-27 residential building sector amounts to 63.6% of the final energy consumption [3]. Across all energy carriers, RES account for 18% of primary energy supply for heating and cooling (H/C), whereas fossil fuels account for the major share of 75% [2].

For Switzerland SH accounts for 65% (145 PJ/yr) of household sector energy use with more than 65% of SH (~100 PJ/yr) covered from fossil fuels. In the Geneva canton, more than 50% of total final energy is used for SH and Domestic Hot Water (DHW) production [4], most of it covered by oil- or gas-fired boilers. Despite the importance of district heating networks (DHN) for a better exploitation of local renewable energy [5–7] only 10% of the total heat market in Geneva is covered by DHN. Based on heating sector

* Corresponding author.
E-mail addresses: alex.daniilidis@unige.ch, a.daniilidis@tudelft.nl (A. Daniilidis).

https://doi.org/10.1016/j.energy.2022.123682
0360-5442/© 2022 The Authors. Published by Elsevier Ltd. This is an open access article under the CC BY-NC license (http://creativecommons.org/licenses/by-nc/4.0/).

importance and the high heat demand density [8], DHN coverage will evolve and should reach 35% of total cantonal heat demand by 2030. Due to new cantonal energy policies, 80% of total DHN production mix should come from waste heat or renewable energies [9]. Therefore, geothermal resources are promising solutions and can represent about 20% of the DHN production mix [10]. The *GEotermies* program developed by Services Industriels de Geneve (the cantonal utility company and energy provider) and the State of Geneva since 2014, is boosting the increase of geothermal energy in the energy system. All types of geothermal energy solutions are implemented, from shallow, low temperature installations using ground source heat pumps to deep project for direct use of hydrothermal resources. Heat storage is being investigated in the European project HEATSTORE.

District Heating and Cooling Networks (DHC) are expanding globally and when the energy supply is produced by renewable energy sources (RES), they can improve sustainability [11,12]. However, few countries have taken advantage of their renewable resource potential for DHC and most networks still rely on fossil fuels [13] with the main barrier being the high initial costs of RES compared to conventional sources. Therefore, significant reductions in CO_2 emissions can be achieved by decarbonizing the heating sector; this is reflected in the increasing global installed capacity and generated energy by direct-use geothermal systems in recent years [14]. Further acceleration in reducing greenhouse gas emissions is planned with the European Green Deal aiming for net-zero GHG emissions by 2050 and decarbonizing the energy sector is a key action point [15].

Low carbon heat sources (e.g., geothermal, biomass, solar and waste-heat) need to be deployed and heat storage plays a pivotal role in this development. Storage provides the flexibility to manage variations in supply and demand of heat at different scales, but especially the seasonal dips and peaks in heat demand. Consequently, Thermal Energy Storage (TES) has seen an increasing amount of research interest in recent years [16]. Aquifer Thermal Energy Storage (ATES) systems are considered a pillar to decarbonize the global energy system [17,18], and mainly in dense urban centres, because of their small surface footprint compared and their ability to cover base load demand [19]. ATES advantages include very large storage potential, shifting of thermal loads in time, low operational costs and high long-term profitability. Planning challenges mainly include proximity between excess heat source, distribution system, suitable aquifer, and end users [20]. Known technical challenges include the high return temperatures of the distribution system, recovery/efficiency factor (ratio between injected and recovered thermal energy) and hydro-geochemical challenges such as precipitation and scaling in wells and pipes.

Low temperature (<30 °C) ATES systems are most common, especially in the Netherlands [21] with around 2500 operating systems for both heating and cooling [22]. Few projects use injection temperatures above 30–40 °C, as only 5 high temperature systems (>60 °C) are currently in operation worldwide [23]. High-Temperature ATES (HT-ATES) systems are attracting an increasing interest amongst industrial operators due to their higher capacity, ability to serve a larger range of temperature levels and limiting HP use for discharging with respect to standard ATES systems [24]. HT-ATES systems models with mono wells achieve efficiencies of up to 70% [25]. The same study identifies the need for demand driven HT-ATES rates. During the 10 first years of exploitation, the Neubrandenburg HT-ATES (doublet well pattern) showed an energy efficiency varying from 40% to 80% with an average value of 56%, with the heating market being the limiting factor [26,27].

A recent review of techno-economic performance of TES systems identified the impact of technical performance on the LCOH and found TES systems to not be competitive with conventional fossil fuel heat sources [28]. However, while techno-economic assessments of low temperature ATES (LT-ATES) systems have been carried out [29], techno-economic assessments of HT-ATES are limited in the literature. Previous studies have highlighted the importance of numerical simulation for characterising performance [30] and identified the lack of economic indicators for HT-ATES systems across Europe, as well as site- and market specific economic analysis [18]. The importance of techno-economic assessment [18,31] and evaluation of CO_2 emission reduction for seasonal thermal energy storage [32] has been recently identified. The reduction of both costs and CO_2 emissions of DH systems using HT-ATES was shown for cities in the Netherlands, however without the use of reservoir simulations [33]. A THM$ study based on analytical formulations has found that a minimum transmissivity of 5×10^{-13} m^3 is required for viable HT-ATES systems [34]. The importance of combined coupling of thermal energy storage (TES), DHN and HPs is also highlighted [35]. However, techno-economic and CO_2 emissions assessment combining fully coupled HT models with DH energy demand has not been performed before in the literature for HT-ATES systems.

We present, for the first time, a new methodology for techno-economic assessment of an HT-ATES system combining subsurface, energy system, operational CO_2 emissions and economic modelling based on a scaled DHN demand. The methodology enables the assessment of HT-ATES contribution to DHN demand, underpinned by HT reservoir simulations and constrained by subsurface properties. The methodology includes an economic model developed to assess the LCOH of the HT simulations and to quantify the avoided CO_2 emissions. The parameters considered include integration strategies (well configuration and cut-off temperature levels) and aquifer parameters (dip, porosity, permeability, depth and thickness and regional groundwater flow conditions). Performance is assessed in terms of capacity, cumulative energy production, Levelized Cost of Heat (LCOH) and avoided CO_2 emissions. Injection rates used by the system are limited by an upper limit of fluid pressure equal to 80% of the overburden to avoid hydraulic fracturing in the formation. Our methodology and analysis is demonstrated with input from HEATSTORE project location in Geneva, Switzerland. Notwithstanding, our study is readily applicable to any location, conditioned to data availability. Results show that a minimum transmissivity of 2.5×10^{-12} m^3 is needed to reach a Levelised Cost Of Heat (LCOH) below 200 CHF/MWh. Additionally, a capacity of 25 MW or higher is required for HT-ATES to become competitive with other large-scale DHN heat sources. The addition of Heat Pumps (HP) results in a capacity increase but also increases LCOH. The methodology presented connects HT-ATES dimensioning based on subsurface constraints, to the DHN for planning purposes. This opens up the possibility for a fully-coupled assessment of DHN and HT-ATES systems in site-specific assessments.

2. Background

2.1. Geological context

Sedimentary basins are attracting geothermal sector interest as they are globally distributed [36] and cover a large portion of densely populated areas where demand for heating and cooling is prominent. For this study, the Molasse basin westernmost part, one of the main sedimentary basins in Europe, covering the Geneva area and known as Geneva Basin (GB), is considered. The GB covers about 2000 km^2 from the town of Nyon to the NE, down to Vuache Mountain to the SW and it is limited by the Jura Haute-Chaine to the NW and by the subalpine nappes to the SE (Fig. 1) [37–39]. In the GB four major lithostratigraphic units of geothermal interest are recorded at depth [40–43]. From bottom to top, these are 1) the crystalline basement including Permo-Carboniferous (PC) troughs at the bottom and its sedime–ntary cover composed respectively of 2) Mesozoic carbonate units which are the focus of this study and, at the top, 3) Cenozoic and 4) Quaternary sediments.

Within the HEATSTORE project, Upper Mesozoic carbonates (Lower Cretaceous and Upper Jurassic) have been identified as a potential target for storing industrial excess heat generated from a waste incineration plant located a few kilometres from the Geneva city. Upper Jurassic is mostly composed of competent, often massive, carbonate deposits, that locally show enhanced porosity values thanks to the presence of biothermal reef facies at its base and to fault corridors that create preferential flow paths for geothermal waters. The Lower Cretaceous, represents the top of the Mesozoic sequence and is composed of fine-grained limestones which can be intensely fractured and highly productive as shown by the GEo-01 exploration well drilling results, where more than 70% of the total flow rate (55 l/s at 34 °C) is discharged from this geologic formation. The Mesozoic unit crop out in the Jura Mountains and dip towards SE where they attain a depth of about

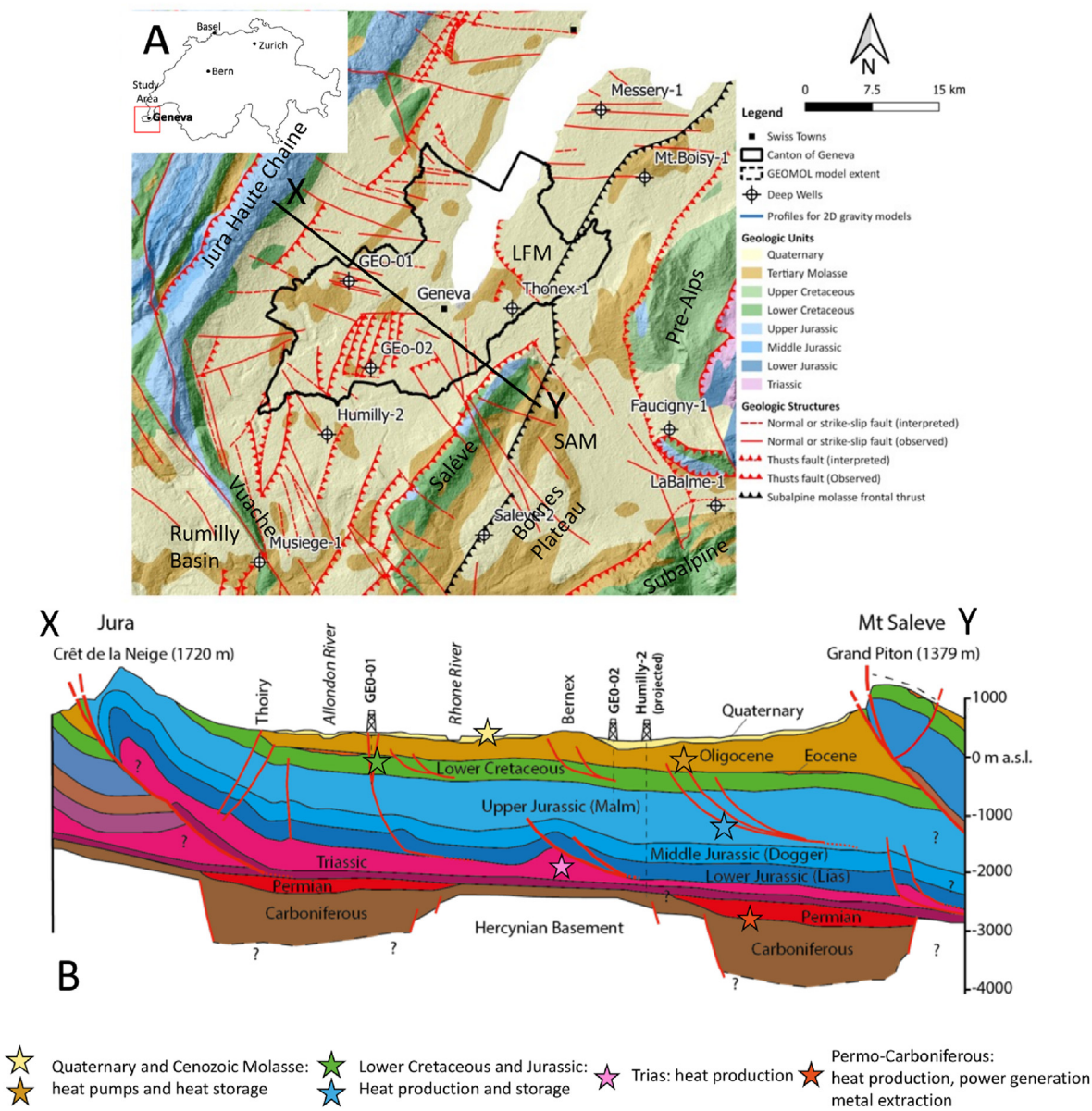

Fig. 1. Map of Switzerland with the location of the study area (a); Geological map over the Geneva Basin with an indication of the main fault structures and deep wells (modified from [40,44] Cross-section cutting through the GGB (modified from [42] indicating the main geothermal targets (c).

1400 m. In order to consider a representative depth for the Geneva subsurface two depth of investigations (500 and 1000 m) were identified for subsurface modelling.

2.2. Geneva HT-ATES project description

The HT-ATES system investigated in the HEATSTORE project is based on subsurface data (geology, geophysics, petrophysics, water geochemistry) produced during the last 3 years and in particular coming from the drilling operations of two exploration wells, completed by SIG in the *GEothermies* program. The GEo-01 and GEo-02 well, targeted the carbonate reservoir in the Upper Mesozoic (Malm and Lower Cretaceous), which are known to be rather tight and low permeable geologic formation but being affected by karstification and locally cut by large fault structures can represent excellent geothermal reservoirs. However, distribution of suitable reservoirs in the explored geologic formations are heterogeneous as demonstrated by the opposite production results achieved at the GEo-01 well (50 L/s from 744 m in depth), GEo-02 (0.6 L/s from 1456 m in depth) and Thonex-01 well (0.3 L/s from 2530 m in depth). Data have been combined in a simplified 3D static model that incorporates the main geologic characteristics representative of the greater Geneva subsurface and that can be adapted to site-specific conditions in the future.

3. Methods and models

Based on hourly measurements at Geneva of an existing district-heating network (430 GWh on 2014 - [5,8]), dimensionless dynamics of a typical DHN heating demand have been created. We assume that renewable energy capacities cover 20% of maximum hourly heat load, which corresponds to cover about 50% of DHN energy demand. The daily averaged heat load average is depicted in Fig. 2a; availability of heat for HT-ATES charging covers the period between May and September (Fig. 2a). HT-ATES capacity was determined based on results from the simulations and constraints therein, while the DHN capacity was scaled accordingly, ensuring a match of available energy for storage. During HT-ATES simulation available heat for charging was not restricted, therefore charge capacity was only limited by subsurface characteristics. HT-ATES operation cycle was 120 days charging, 60 days rest and 120 days discharging followed by 65.25 days rest (Fig. 2b), repeated yearly for 15 years of total simulated time. Representative yearly charging and discharging cycles are shown in normalized values in (Fig. 2b).

3.1. Energy demand models

Energy studies were based on Geneva's values for future DHN evolution. Geo-referred final energy consumption for heating is available at building level in a public database [45]. Based on this geospatial information, the public-owned energy provider (SIG) planned future facilities and associated production to answer increasing grid heat demand and ensure a minimum share of renewables (~80%). An hourly input-output model inspired from EnergyPLAN [46] was used to design heat power capacity of different plants and evaluate annual heating network production mix [10] (Fig. 2a).

A production merit-order has been chosen based on direct CO_2 emissions and energy consumption, waste heat recovery is used to cover the base load while wood and gas boilers are activated to ensure peak production. High temperature HPs have also been used to increase local renewable resources temperature (geothermal, lake and sewage water). Higher source temperatures, received a higher priority, since HP's electric consumption is proportional to

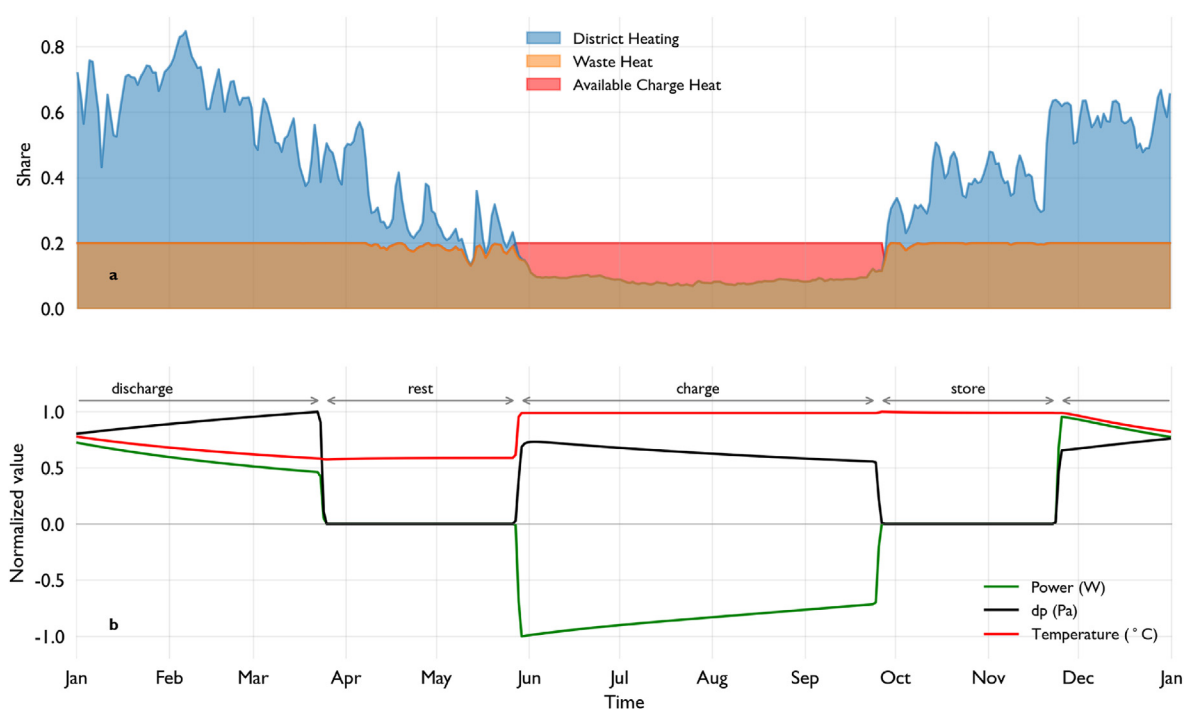

Fig. 2. Daily averages for district heating demand, waste heat and available heat for charging (a) HT-ATES indicative yearly production scheme normalized to unit value (a). Negative power corresponds to charging and positive power to HT-ATES discharging. During discharge, production temperature gradually drops until either the discharge period ends or the cut-off temperature is reached. Due to this temperature reduction produced fluid density decreases resulting in increasing pressure difference. During charging, if the warm fluid from the hot well affects the cold well, a slight drop in system power can be observed. Data shown for the simulation with aquifer thickness 50 m, aquifer permeability 1×10^{-13}, aquifer porosity of 10%, two wells (doublet), no groundwater velocity, a 15° aquifer dip, a temperature cut-off of 20 °C and an aquifer depth of 1000 m. The DHN heat share is lower than 1 due to daily averaging of underlying hourly heat demand data. District heating demand and waste heat availability are detailed in Section 3.1.

the difference between source and sink temperatures [47,48]. HT-ATES was activated after waste heat recovery, before large-scale HP, with HT-ATES energy being directly injected into the DHN while its temperature is higher than the DHN return temperature.

By 2035, HT-ATES charging energy might range from 20 GWh/yr. to more than 60 GWh/yr. depending on charging strategy and facility dimensioning (power limitation); based on the chosen merit-order, future DHN could accept up to 600 GWh/yr. and 290 MW from HT-ATES [49]. From these values and based on local geological conditions, thermo-hydraulic simulations were made. To characterise maximum aquifer potential the energy amount available for storage was not constrained. Injected and extracted flowrates were in turn only constrained by mechanical assumptions, while charging/discharging process could have been interrupted by temperature cut-off on the DHN/HT-ATES interface (see §3.2).

3.2. Thermo-hydraulic simulations

Thermo-hydrolic simulations were carried out using state of the art 3D porous media flow reservoir simulator Nexus-CSMP++ [50]. Modelled characteristics included both forced and natural convective processes, instantaneous exchange of heat between rock and fluid, and an accurate state for water via the IAPWS standard formulation IAPS-84 [51] and the IAPWS-R12-08 model for water viscosity [52]. Porous rock material properties were assumed isotropic, locally uniform to a minimum discrete level of a computational cell, and constant. Kinetic, potential, and viscous dissipation effects were neglected.

Data used consist of a set of simulation scenarios generated and used by Ref. [53] to perform a sensitivity study of a simplified HT-ATES system to a set of pre-established key characteristics (see Table 1). Here we include 1152 scenarios simulated to answer first stage feasibility and design questions related to geology, hydrology, and system operation. Parameters varied include hydro-geologic aquifer properties of thickness, permeability, porosity, depth, dip, artesian conditions, and groundwater hydraulic gradient, as well as the operational ones of well pattern and cut-off temperature. Simulation results are used here as input to a combined economic and CO_2 emissions analysis. For a more detailed explanation of setup, initial conditions, system boundaries, governing equations and thermo-hydraulic simulation results the reader is referred to Ref. [53].

In absence of artesian conditions, pressure was assumed to increase with depth following a hydrostatic gradient. Horizontal groundwater flow in the x-direction, when present, was simulated via a pressure differential between two opposing y-z plane model boundaries. The resulting groundwater flow velocity was mainly dependent on aquifer permeability. Artesian conditions were represented via a 1 MPa increase in reference pressure set at the top model boundary. A temperature profile was constructed to establish initial conditions, based on a surface temperature of 10 °C and an averaged continental heatflux of 64 mW/m^2 [36]. When modelling deeper aquifers, both reference pressure and temperature at the top boundary were altered accordingly, to 6 MPa and 25 °C, respectively, following the respective hydrostatic pressure gradient (with artesian conditions where appropriate) and continental heat flux.

In all simulations, the flow rate used was identical in both charge and discharge operation modes, and was assumed to be the maximum possible given the conditions of permeability, depth, thickness (i.e. available screen length), and whether artesian conditions were present. The underlying premise consisted in preventing fluid pressure exerted by wells to exceed hydro-fracture (HF) failure conditions, considered as 80% of overburden pressure at the reservoir depth for injection, and above cavitation conditions for production.

HT-ATES charging was carried out with a temperature of 90 °C for all simulations. A value of cut-off temperature (see Table 1) was used for two main purposes: a) to calculate exergy values and thus measure the usefulness of energy charged and discharged, b) to trigger an operational mode change when the ATES was in discharge mode. In the latter situation, the system went into rest mode if the output temperature from the main/hot well dropped below the cut-off temperature. Cut-off temperature values were selected to be aligned with DHN required temperature without (50 °C) and with the use of a HP (20 °C) (see also §3.3).

We defined complete ATES system instantaneous power P as:

$$P = \int_{\Gamma_{MW_1}} q_{MW_1}\, d\Gamma + \sum_{j=1}^{N_A} \int_{\Gamma_{AUXW_j}} q_{AUXW_1}\, d\Gamma \tag{1}$$

where q_{MW_1} is the instantaneous flow of heat through the main well per unit area, q_{AUXW_j} is the instantaneous flow of heat per unit area through auxiliary well j of N_A number of auxiliary wells, and Γ defines a closed surface that surrounds each well in close proximity. Analogously, instantaneous exergetic power P_χ is defined as [54]:

$$P_\chi = \int_{\Gamma_{MW_1}} q_{MW_1}\left(1-\frac{T_{CO}}{T}\right) d\Gamma + \sum_{j=1}^{N_A} \int_{\Gamma_{AUXW_j}} q_{AUXW_1}\left(1-\frac{T_{CO}}{T}\right) d\Gamma \tag{2}$$

where T_{CO} is cut-off temperature, T is temperature measured at the surface being integrated (Γ), and both are measured in Kelvin. We therefore can define lifetime-averaged energy and exergy efficiencies, η and η_χ, as:

$$\eta = \frac{1}{N_C}\sum_{n=1}^{N_C} \frac{-\int_{t_{Dn}}^{t_{Dn}+\Delta t_{Dn}} P\, dt}{\int_{t_{Cn}}^{t_{Cn}+\Delta t_{Cn}} P\, dt} \qquad \eta_\chi = \frac{1}{N_C}\sum_{n=1}^{N_C} \frac{-\int_{t_{Dn}}^{t_{Dn}+\Delta t_{Dn}} P_\chi\, dt}{\int_{t_{Cn}}^{t_{Cn}+\Delta t_{Cn}} P_\chi\, dt} \tag{3}$$

where N_C is the number of cycles in the system lifetime (i.e. 15, in years), t_C and t_D are the times that mark the beginning of charging and discharging stages, respectively, and Δt_C and Δt_D are the corresponding durations of charging and discharging stages, respectively.

Table 1
Parameters and values used in reservoir simulations. A factorial design for all parameters is used resulting in 1152 3D reservoir simulations. All simulations use a temperature of 90 °C for HT-ATES charging and a well spacing of 141 m.

Parameter	Value	Units
Aquifer thickness	50, 100, 150	m
Aquifer permeability	1×10^{-14}, 5×10^{-14}, 1×10^{-13}	m^2
Aquifer porosity	10, 20	%
Well pattern	Doublet, 5-spot	–
Cut-off temperature	20, 50	°C
Aquifer depth	500, 1000	m
Aquifer dip	0, 15	°
Groundwater hydraulic gradient	0, 51.7	%
Artesian conditions	0, 1	MPa

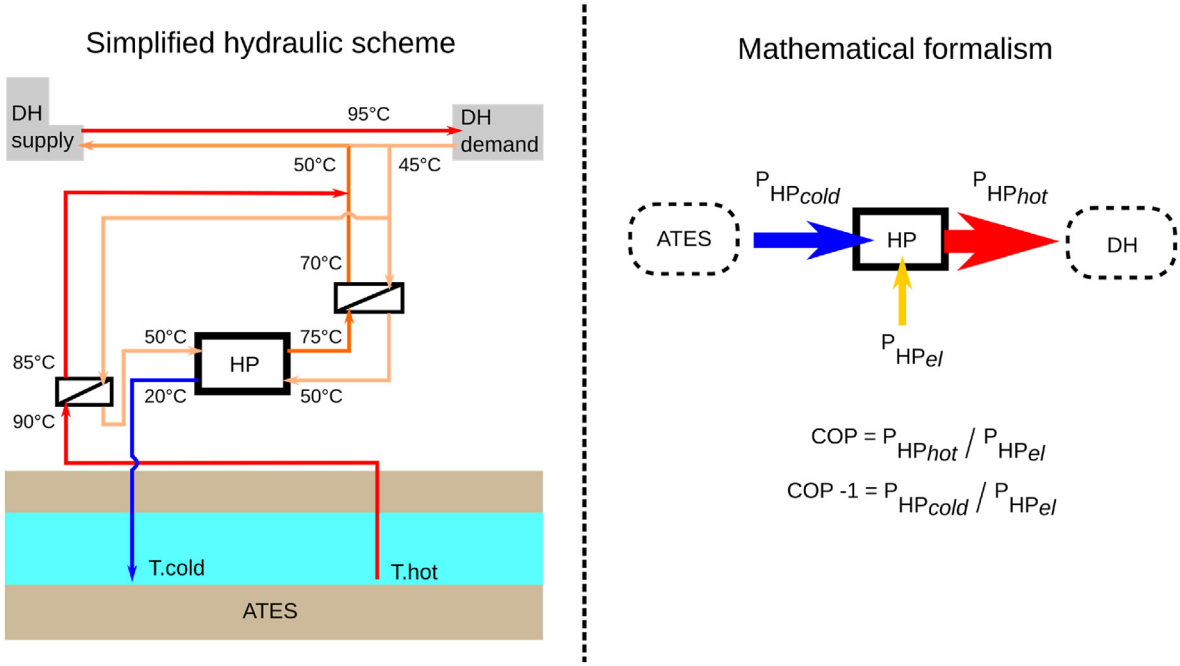

Fig. 3. HT-ATES and HP integration schematic representation integration for the case of 20 °C re-injection temperature and the respective energy conversions related to the HP. Notice that to enhance the system efficiency, the HT-ATES and the HP production are injected in the DHN return branches.

3.3. Discharge strategy

During discharge, two different cold temperatures were simulated, 50 °C or 20 °C. The 50 °C temperature on the cold well represents direct use of heat. In this case, heat was transferred from the HT-ATES hot well to the DHN by a heat exchanger. For the 20 °C temperature simulated HPs were used to increase the energy extracted from the storage. After a direct use of heat, the geothermal water temperature was cooled down by a series of HPs before been re-injected into the aquifer (Fig. 3). A similar system is in place since 1994 in Riehen, Switzerland (Faessler and Lachal, 2017). This assisted heat extraction enabled production of heat at a higher temperature and also the extraction of more energy from the aquifer since the temperate difference between the cold and the hot well was increased when compared to a direct use of heat.

HPs were assumed to have a constant COP of 3, even though it is widely known that the COP is dependent on the cold source temperature. This simplification was done because i) after using heat directly, HP inlet temperature is limited to the range 50 °C–20 °C; ii) the amount of HP extracted energy from the ATES is independent from COP assumptions (see below); and because iii) this relatively low COP can be seen as a worst-case scenario for electricity consumption., a COP of 6 would reduce HP electricity consumption by 60%.

Electrical power (MW) for HPs operation was computed as:

$$P_{HP_{el}} = \frac{P_{HP_{cold}}}{(COP - 1)} \tag{4}$$

where $P_{HP_{cold}}$ is the available power on the cold side of the HP (MW) and can be evaluated based on the temperature drop from 50 °C to 20 °C. This is equivalent to subtracting, at each time step and for a defined set of reservoir parameters, the available power for the 20 °C re-reinjection scenario and the extracted power from the storage when re-injection temperature is set to 50 °C.

The HP thermal power dimensioning, necessary for the economic analysis, was set as the maximum electric power needed ($P_{HP_{elmax}}$) during the 15 yr of exploitation times the system COP:

$$P_{HP_{th}} = P_{HP_{elmax}} COP \tag{5}$$

3.4. Economic assessment

HT-ATES pumping requirements were computed according to:

$$P_{pump} = \frac{q\sum_{k=1}^{N_w}\left(\left|P - P_{ref}\right|\right)}{\eta_{pump}} \tag{6}$$

where q is the volume flow rate (m^3/h), N_w is the number of wells, P is well pressure, P_{ref} is the aquifer reference pressure when no pumping takes place and η_{pump} is the pump efficiency. It should be noted that this pressure difference was computed per each well according to the well strategy used. Required pumping power was the pumping power sum of for all wells.

Drilling costs were computed with the use of an analytical formula based on the drilling cost per depth provided of the Netherlands [55], adjusted to fit the few data points for drilling costs available for Switzerland:

$$C_{well} = 1480000 + 1150Z + 0.3Z^2 \tag{7}$$

where Z is the measured depth. Capital Expenditures were computed according to:

$$CapEx_t = C_{well}N_w + C_{facilities} + C_{HP} + \sum_{t=0}^{n} C_{pump}N_wR_t \tag{8}$$

where C_{well} is the well drilling cost, $C_{facilities}$ is the ATES required surface facilities cost required, C_{HP} is the HPs cost, C_{pump} is the pump cost, N_w is the number of wells drilled and R_t is the time instance at which the pumps are replaced. Operation Expenditures

Table 2
Economic analysis inputs.

Parameter	Value	Unit	Reference
Facilities costs	10	% of drilling costs	
Electricity price	120	CHF/MWh	[56]
Waste heat price	35	CHF/MWh	[57]
Discount rate	5	%	
OpEx % CapEx	3	%/y	[56]
Drilling costs	Eq. (7)	CHF	Modified after [55]
Pump cost	500	kCHF	
Pump replacement	5	Years	
Discharge cycle pump efficiency	40	%	
Charge cycle pump efficiency	50	%	
HP cost	800	kCHF/MW	[58]
HP COP	3	–	

were computed according to:

$$OpEx = OpEx_{\%} \sum_{t=0}^{n} CapEx + \sum_{t=0}^{n} \sum_{1}^{N_w} P_{pump} El_{price} \tag{9}$$

where $OpEx_{\%}$ is the OpEx as a percentage of CapEx per year and El_{price} is the electricity price. Levelized Cost of Heat (LCOH) is computed according to:

$$LCOH = \frac{\sum_{t=0}^{n} \frac{CapEx_t + OpEx_t + CH_t}{(1+r)^t}}{\sum_{t=0}^{n} \frac{E_t}{(1+r)^t}} \tag{10}$$

where CH_t is the charge heat cost, r is the discount rate, t is the elapsed number of time periods, E_t is the energy extracted during time period t and n is the total number of periods considered. Economic assessment inputs are summarized in Table 2.

3.5. DHN integration

The HT-ATES system was modelled without any limitation to the available energy used for charging. Therefore, the DHN that it could contribute to should have at least that amount of energy available for storage. This was introduced via a scaling factor, that scales the DHN network capacity based on the required energy for charging each HT-ATES simulation. For simplicity, we ignored minor, short-term differences (7 days window) at the beginning of the charging cycle between the available heat for charging and ATES stored energy, that amounted to less than 1.3% of charged energy per cycle. The scaling factor was calculated during the charge period (Fig. 2) where the DHN power demand is lower than the available waste heat and therefore there is enough energy for charging the storage. The scaling factor was calculated as:

$$DH_{scale} = \frac{HTATES_{charge_{nom}}}{min\left(WH_{mode} - DHN_{charge}\right)} \tag{11}$$

in which $HTATES_{charge_{nom}}$ is the ATES nominal charging capacity (MW), min is the minimum value WH_{mode} is the waste heat mode value (fixed to 0.2 of maximum DHN demand) (ratio) and DHN_{charge} is the DHN demand over the HT-ATES charge period (ratio). HT-ATES energy contribution share (including HPs where appropriate) was calculated as:

$$HTATES_{share} = \frac{\sum_{t=0}^{n} HTATES_{E_{th}}}{\sum_{t=0}^{n} DH_{E_{th}}} \tag{12}$$

where $\sum_{t=0}^{n} HTATES_{E_{th}}$ is the HT-ATES cumulative energy (MWh) generated including the HP energy where appropriate and $\sum_{t=0}^{n} DH_{E_{th}}$ is the district heating cumulative energy (MWh) demand over 15 years. Due to the choice of ensuring that sufficient energy for HT-ATES charging was available throughout the whole charging period, not all the available heat for charging was utilized by the HT-ATES system. Therefore, our energy share results can be considered as a conservative estimate of HT-ATES contribution.

3.6. CO_2 emissions

Operational CO_2 emissions balance was analysed based on current electricity CO_2 intensity data. The avoided CO_2 emissions include system operation and did not consider the wells installation and other equipment required in ATES system commissioning. HT-ATES operational CO_2 intensity was given by:

$$HTATES_{CO_2} = \sum_{t=0}^{n} HTATES_{E_{el}} C_{el} - \sum_{t=0}^{n} HTATES_{E_{th}} C_{gas} \tag{13}$$

where $HTATES_{E_{el}}$ is the energy (MWh) required for HT-ATES pumps and HPs operation, C_{el} is the electricity mix CO_2 intensity, $HTATES_{E_{th}}$ is the HT-ATES provided heating energy (MWh) provided and C_{gas} is the CO_2 intensity of gas heat currently provided to the DHN network that the HT-ATES system is replacing. The latest national Swiss database for CO_2 intensity per source was used as a reference [59] according to Table 3.

Table 3
CO_2 intensity values used.

Electricity intensity scenario	CO_2 intensity [59]
Electricity High (CHP biogas)	0.177 kg CO_2 eq/kWh
Electricity Mean (CH mix)	0.102 kg CO_2 eq/kWh
Electricity Low (geothermal CHP)	0.031 kg CO_2 eq/kWh
Gas heat (provided by DHN)	0.3140 kg CO_2 eq/kWh

4. Results

Results present firstly the nominal capacity sensitivity followed by LCOH and avoided CO_2 emissions to the inputs. The next subchapter discusses LCOH as a function of HT-ATES efficiency. Lastly, HT-ATES contribution to energy demand is presented. An indication of temperature distribution after 15 years of operation is presented in Appendix A for a two well and five well pattern.

4.1. Sensitivity to inputs

4.1.1. Dimensioning

Nominal HT-ATES discharge capacity together with HP spans a range between 0.4 MW and 81 MW and is mostly controlled by aquifer permeability, with higher permeability resulting in significantly higher nominal capacity (Fig. 4b). Notably, a low permeability of 1×10^{-14} m^2 results in nominal discharge capacity below 8 MW under all other parameters tested. Higher nominal discharge capacity is reached with thicker aquifers and higher permeability (Fig. 4a). Cut-off temperature reduction results in nominal capacity increase since the extractable amount of heat is higher due to the increased temperature difference and HP contribution (Fig. 4e). A deeper aquifer increases nominal capacity by raising the pressure threshold for injection, due to the higher lithostatic pressure, and also aquifer temperature (Fig. 4f). Artesian conditions of 1 MPa slightly improve on the nominal capacity compared to no artesian conditions by increasing the pressure headroom available for storage (Fig. 4i). Artesian condition increases for systems with higher nominal capacity. Aquifer porosity, number of wells, aquifer dip and presence of a hydraulic gradient do not impact HT-ATES nominal discharge capacity (Fig. 4c, d,g&h respectively).

4.1.2. LCOH

LCOH is primarily affected by aquifer permeability. For a high permeability of 1×10^{-13} m^2 LCOH remains below circa 600 CHF/MWh at all times, while for low permeability of 1×10^{-14} m^2 LCOH increases beyond 5000 CHF/MWh (Fig. 5b). A less thick aquifer results in a significant increase in LCOH, while for an aquifer

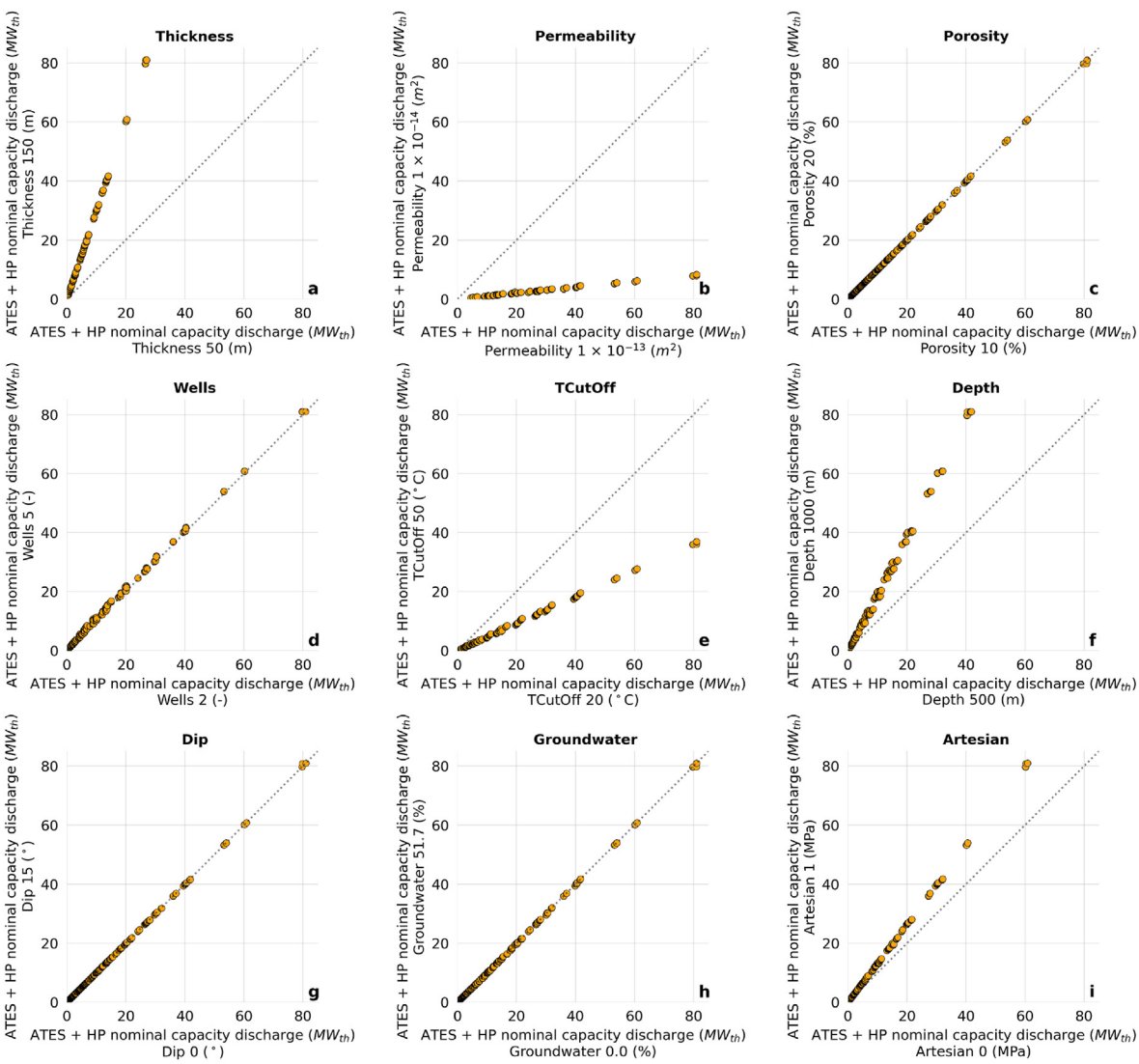

Fig. 4. Parameters affecting HT-ATES nominal discharge capacity. The subplots show the change in nominal discharge capacity for each highest and lowest value of the respective input parameter in the title, with all other parameters being identical for each point plotted. Dashed line represents an ideal one-to-one ratio between the two values; therefore, points plotted along the dashed line imply no change is introduced in the metric by altering the parameter value. All inputs show a linear relation in terms of nominal capacity.

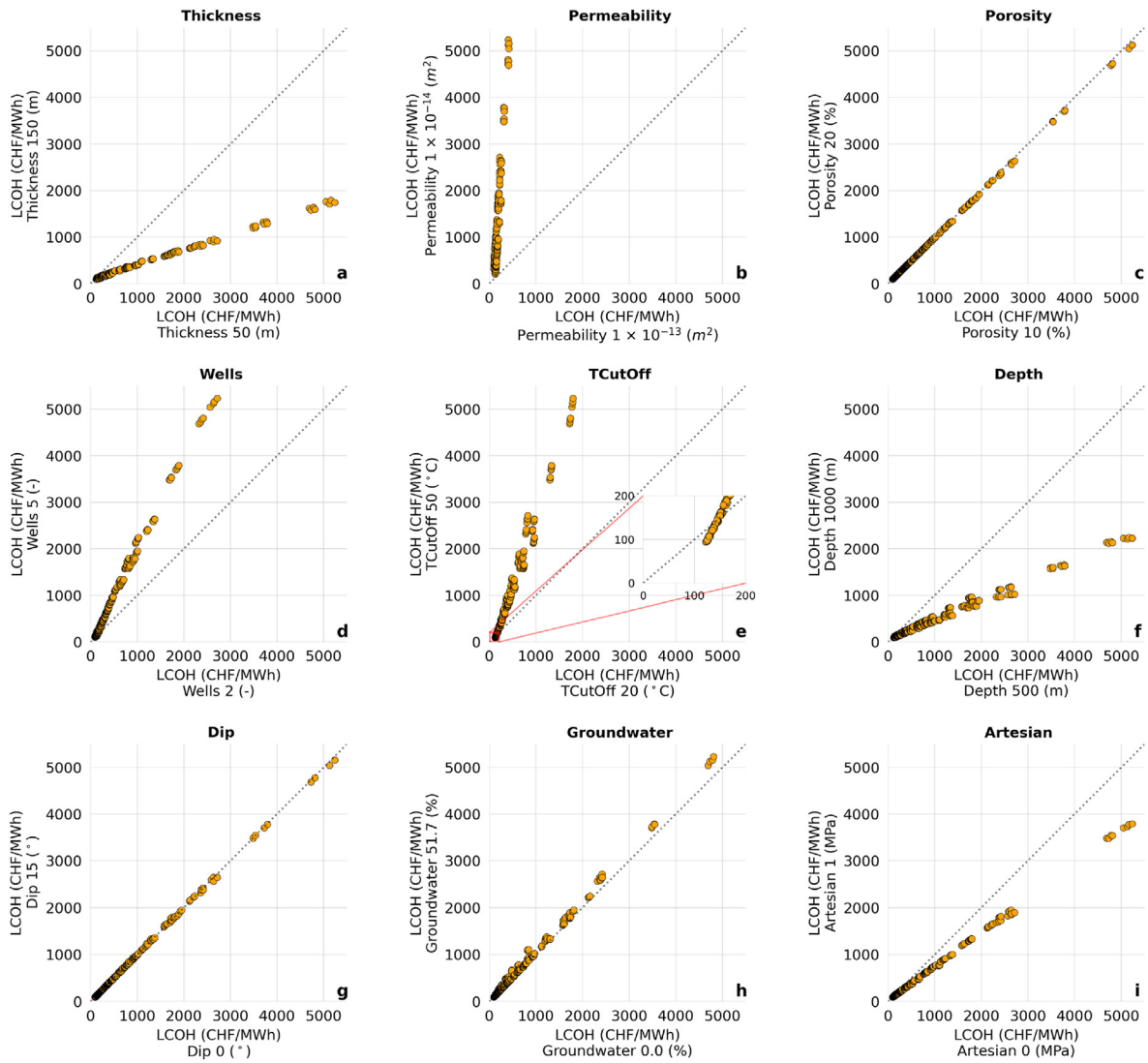

Fig. 5. Parameters affecting LCOH. Subplots show the change in LCOH for each highest and lowest value of respective input parameter in the title, with all other parameters being identical for each point plotted. Dashed line represents an ideal one-to-one ratio between two values; therefore, points plotted along the dashed line imply no change is introduced in the metric by altering the parameter value.

thickness of 150 m LCOH remains below 2000 CHF/MWh (Fig. 5a) regardless of other parameter values. A cut-off temperature of 20 °C yields an LCOH that is lower than for 50 °C (Fig. 5e, see also Fig. 6) for most simulations. However, this trend is reversed for systems that achieve an LCOH below circa 150 CHF/MWh (Fig. 5e inset axes). When conditions are favourable, a cut-off temperature of 50 °C result in lower LCOH due to avoiding HP related costs. A deeper aquifer decreases LCOH but the relation here is not completely linear and two separate trendlines appear (Fig. 5f). Additional well costs required in the 5-spot configuration does not offset pumping costs (pumps and operational costs for pumping) and therefore increases the HT-ATES LCOH (Fig. 5d). Artesian conditions reduce LCOH by increasing the nominal capacity slightly due to higher-pressure threshold as previously discussed (Fig. 5i). Groundwater flow due to a hydraulic gradient slightly increases LCOH, by reducing aquifer efficiency in storing and recovering heat (Fig. 5h). Aquifer porosity and dip do not affect LCOH (Fig. 5c&g respectively).

LCOH as a function of nominal discharge capacity shows an inverse relationship, with higher nominal capacity resulting in lower LCOH (Fig. 6a). Notably, a large number of simulations achieve a similar nominal capacity but span a very large range of LCOH for capacities up to circa 5 MW (Fig. 6a). LCOH spread is reducing as the

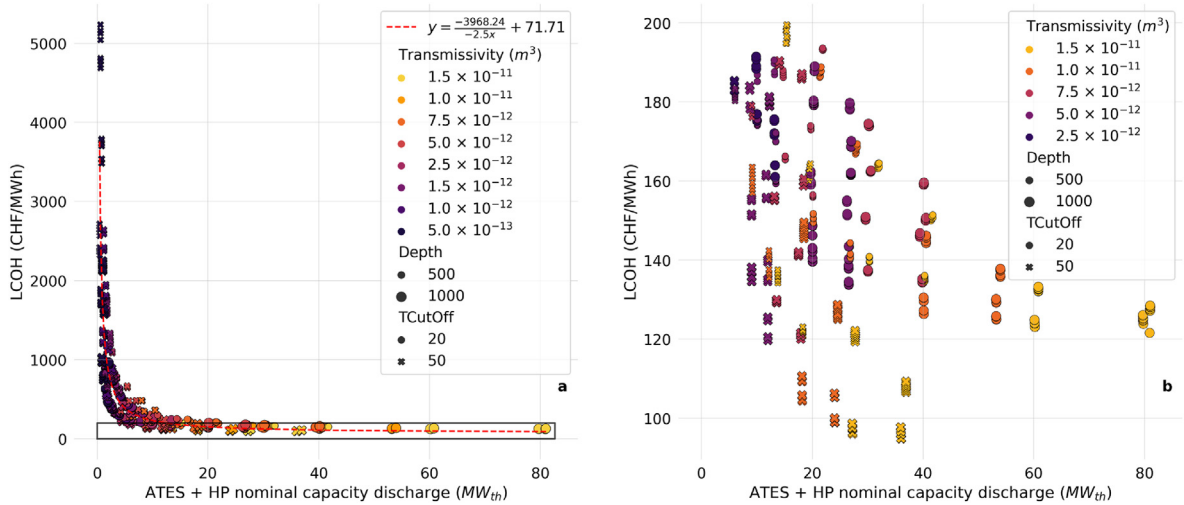

Fig. 6. LCOH against nominal production capacity coloured by reservoir transmissivity, sized by depth and marked by temperature cut-off (a). The dashed line in the left-hand figure (a) outlines right-hand side figure extent (b).

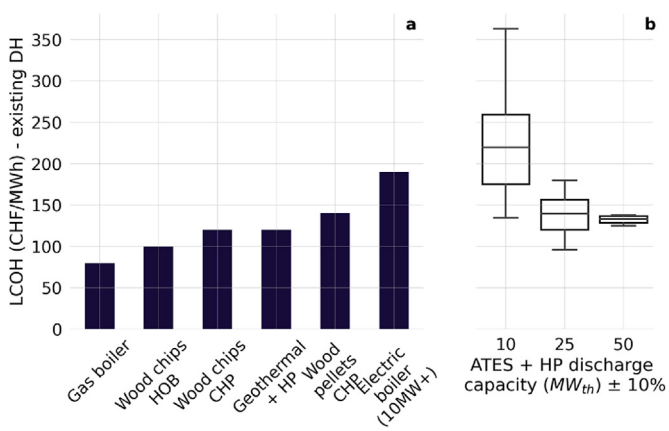

Fig. 7. LCOH for other energy technologies providing heat to a DHN (a) and distribution of results from for HT-ATES from this study (b). Data source [60].

nominal capacity increases further and reduces to circa 130 CHF/MWh above a capacity of 40 MW. For simulations that resulted in an LCOH lower than 200 CHF/MWh (Fig. 6b), a minimum transmissivity is of 2.5×10^{-12} m^3 is required. Additionally, we observe that a cut-off temperature of 20 °C reached a lowest LCOH value of circa 120 CHF/MWh for the most favourably transmissivity of 1.5×10^{-11} m^3 and a nominal discharge capacity of circa 80 MW (Fig. 6b). Comparably, simulations with a cut-off temperature of 50 °C and a transmissivity of 1.5×10^{-11} m^3 achieve LCOH values as low as circa 90 CHF/MWh, at nominal discharge capacity >35 MW (Fig. 6b).

With respect to other energy sources for heating [60], the studied HT-ATES system (Fig. 7) starts to be comparable when nominal capacity is above circa 10 MW. To become competitive, HT-ATES systems require capacities ≥25 MW to achieve a median LCOH below 165 CHF/MWh and requires a transmissivity of at least 7.5×10^{-12} m^3 (Fig. 6b).

4.2. LCOH and HT-ATES efficiency

Energy against exergy efficiency after 15 years of HT-ATES operation shows a linear relationship for the cut-off temperature of 50 °C (Fig. 8a). A slight deviation from this linear behaviour is observed towards better energy efficiencies as the energy efficiency increases and deeper systems are used (Fig. 8a). For a cut-off temperature of 20 °C higher energy efficiency is achieved compared to exergy efficiency, with deeper systems exhibiting further energy efficiency improvement and values reaching close to 100% (Fig. 8a). A large spread in LCOH for similar energy efficiency values is evident for low permeability aquifers (Fig. 8b). This spread decreases with increasing permeability. A similar trend is observed with deeper systems that further improve efficiency and reduce LCOH. Therefore, with favourable conditions a correlation is observed between higher efficiency and lower LCOH (Fig. 8b).

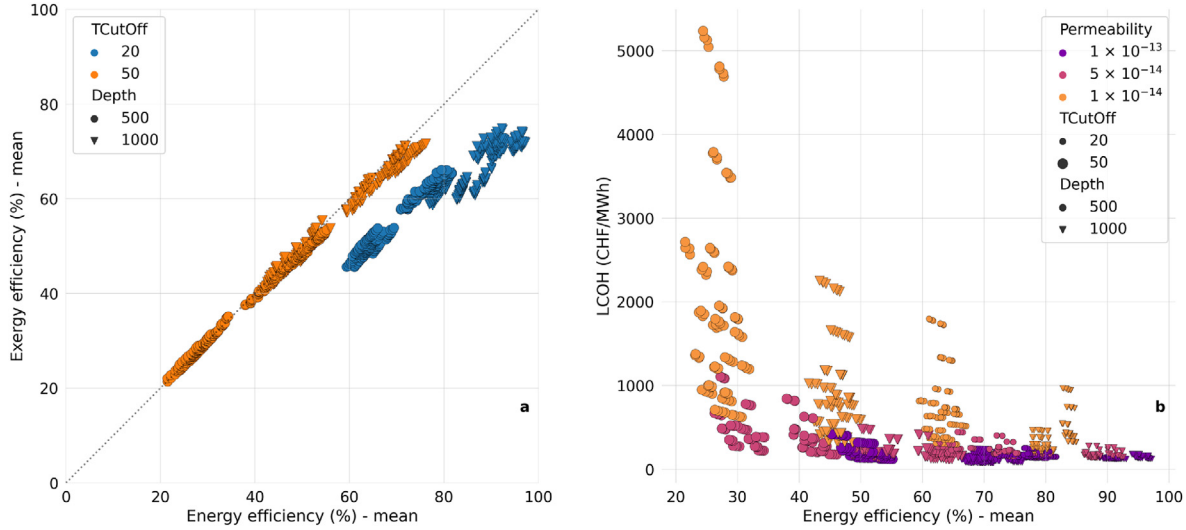

Fig. 8. Mean HT-ATES energy vs exergy efficiency after a 15-year cycle, color coded based on cut-off temperature and marked according to depth (a) and energy efficiency vs LCOH color coded based on permeability, sized according to cut-off temperature and marked according to depth(b).

4.3. Energy share

HT_ATES energy contribution combined with the use of a HP is depicted in Fig. 9. During the charging cycle, the amount of available waste heat is not fully utilized, resulting in circa 25.6% of available waste heat not being used for charging (Fig. 9). Unused waste heat is a result of scaling the DHN based on initial amount of waste heat available for charging, ensuring that sufficient heat is available HT-ATES charging over the charging period duration (see Section 3.5). Therefore, this energy share can be considered as a conservative estimate. The gradual temperature drop during discharge is observed in the form of a decreasing direct discharge with time (green line). The example shown here uses a cut-off temperature of 20 °C; for the 50 °C cut-off temperature the HP contribution and related costs would not be present.

HT-ATES contribution to the energy mix (plus the HP contribution where present) as a total energy demand percentage is dominantly affected by the cut-off temperature in combination with the aquifer depth (Fig. 10e&f). A depth of 1000 m and a cut-off temperature of 20 °C results in an energy share of at least 11% while the same cut-off temperature at a depth of 500 m results in a share of circa 8%. Permeability is a second important factor with high permeability leading to higher system capacity (Fig. 7b) and better energy share percentages (Fig. 10b). Lower energy share is reached

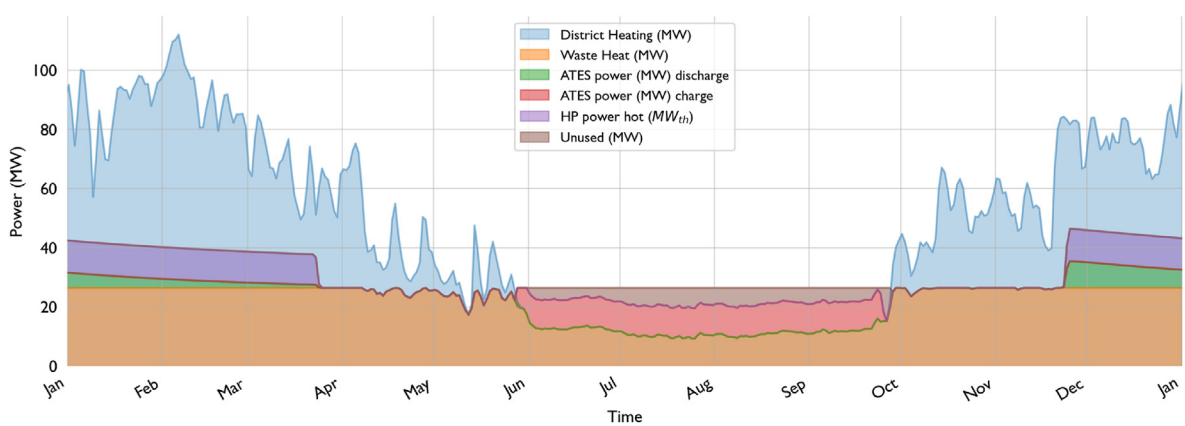

Fig. 9. Example simulation result over a year, showing the amount of heat stored and produced by the HT-ATES system and the HP, the waste heat available and district heating demand. Simulations specifications are: aquifer thickness of 50 m, a doublet well design, no groundwater, 10% aquifer porosity, 15° dip, cut-off temperature of 20 °C and a depth of 1000 m, well spacing of 141 m. The unused part of waste heat amounts to 25.6% of the available waste heat during the charging period.

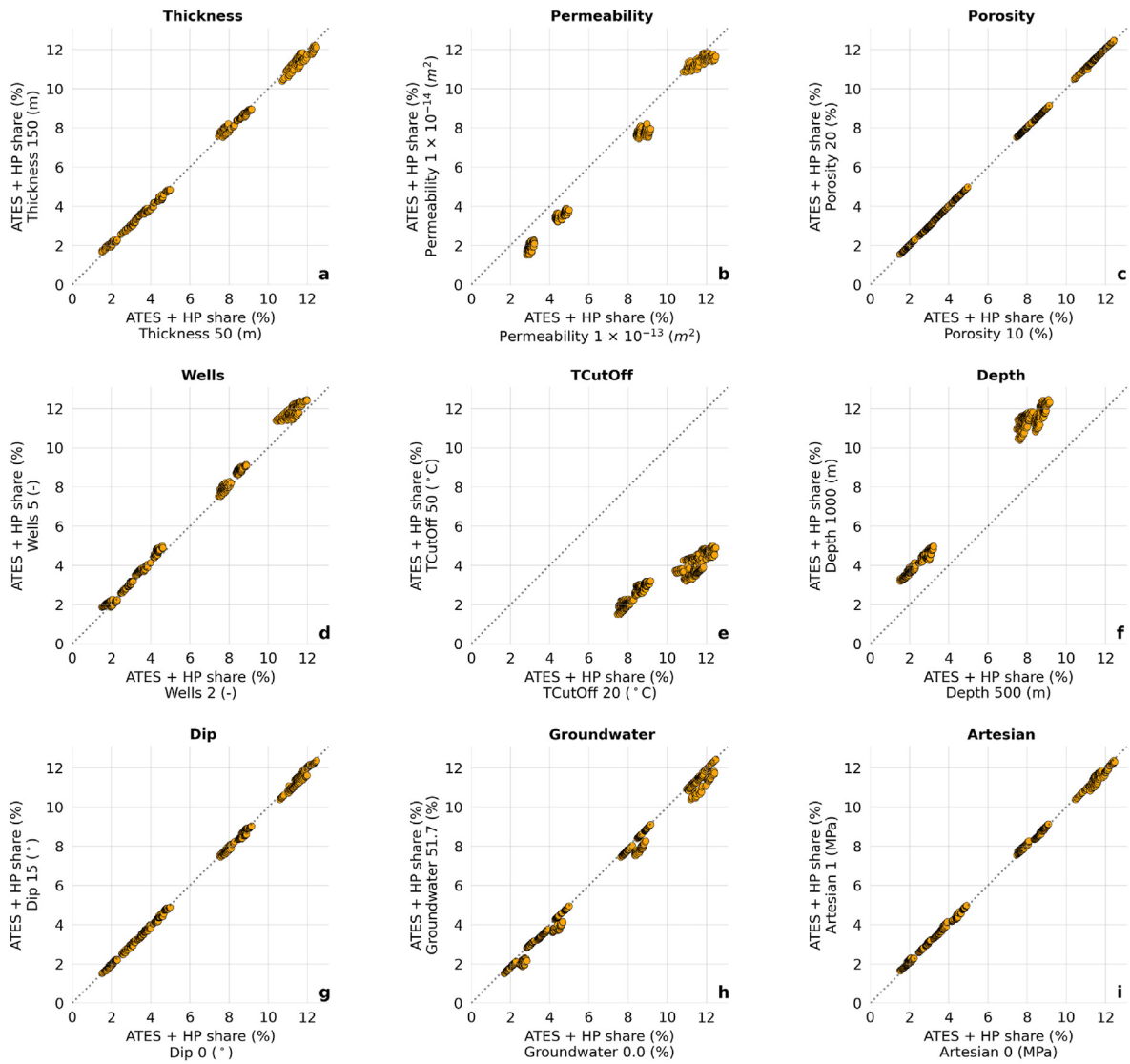

Fig. 10. HT-ATES share sensitivity in overall energy demand over 15 years of operation. Subplots show the change in energy share for each highest and lowest value of the respective input parameter in the title, with all other parameters being identical for each point plotted. Dashed line represents an ideal one-to-one ratio between two values; therefore, points plotted along the dashed line imply no change is introduced in the metric by altering the parameter value.

with a 50 °C cut-off temperature (Fig. 10e). For the cut-off temperature of 20 °C small perturbations can be seen but the higher permeability only leads to small HT-ATES share increases to the energy mix. This is due to sensitivity to depth, where for a 50 °C cut-off temperature an aquifer depth of 1000 m increases the HT-ATES share (Fig. 10f). For the 20 °C cut-off temperature aquifer depth shows a much smaller improvement with deeper aquifers (Fig. 10f). The well number only slightly affects the HT-ATES energy share with a higher shared observed for the five wells configuration and 20 °C cut-off temperature (Fig. 10d). Groundwater flow results in slightly lower energy share (Fig. 10h) due to reduced efficiency in recovering stored heat. Parameters of aquifer thickness, aquifer porosity, aquifer dip, hydraulic gradient, and artesian conditions do not affect energy mix contribution (Fig. 10a,c,g,h&i respectively).

4.4. Avoided CO_2 emissions

Cumulative avoided CO_2 emissions and HT-ATES and HP energy share are controlled largely by cut-off temperature (Fig. 11) as this directly affects nominal system capacity (see also Fig. 4). HT-ATES contribution with a cut-off temperature of 50 °C is affected more by aquifer depth than transmissivity or artesian conditions. For a cut-off temperature of 50 °C, an aquifer depth of 500 m results in an ATES share below 3% and at least 3% for an aquifer depth of 1000 m

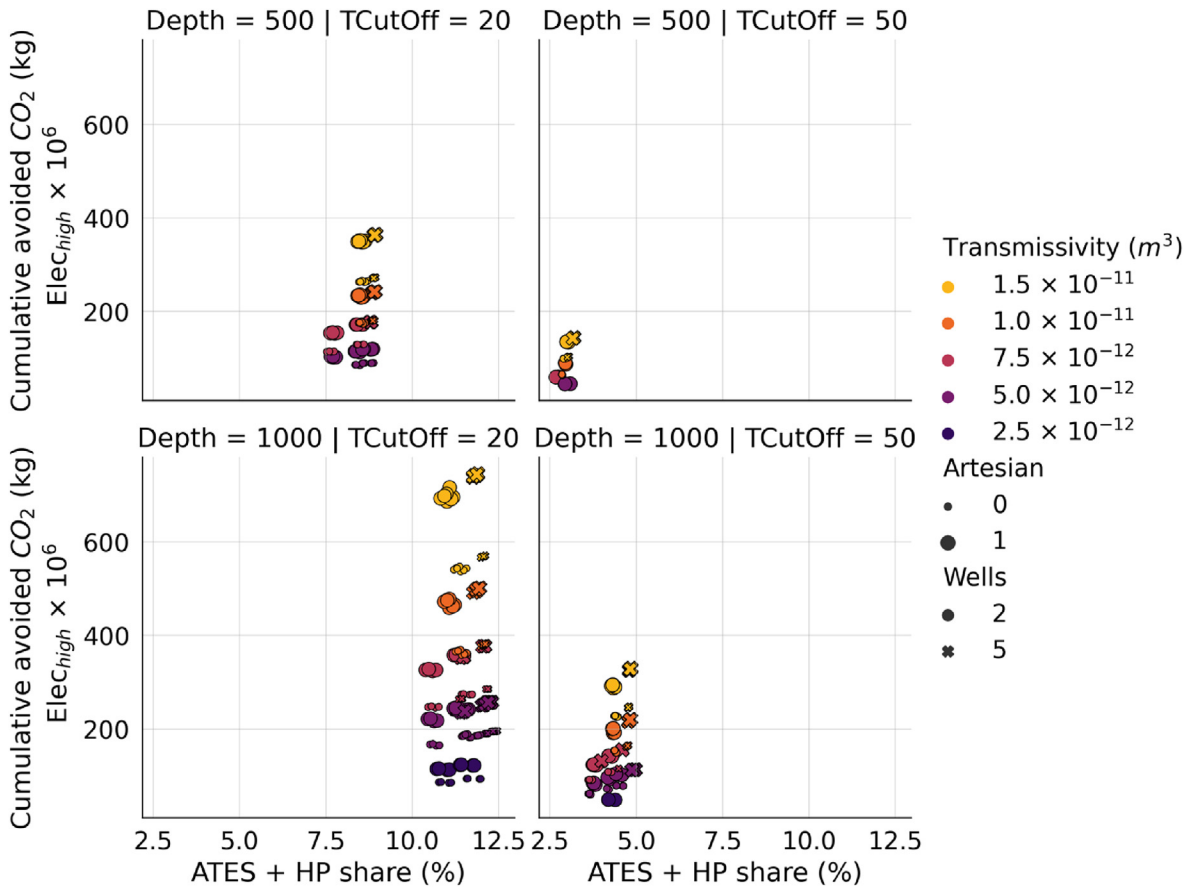

Fig. 11. ATES share and cumulative avoided CO_2 emissions for simulations with an LCOH below 200 CHF/MWh. It should be noted that a cut-off temperature of 50 °C implies that no HP is used in the system.

(Fig. 11). For a cut-off temperature of 20 °C aquifer depth affects the ATES share similarly, from circa 7.5% at 500 m depth to circa 10.5% at a depth of 1000 m. However, the amount of avoided CO_2 emissions increases strongly with deeper systems and almost doubles for systems with a transmissivity of 1.5×10^{-11} m^3 and artesian conditions (Fig. 11). Deeper systems with a cut-off temperature of 20 °C result in avoided emissions are in excess of 0.7 billion kg of CO_2 equivalent when high electricity grid CO_2 intensity is used (worst case scenario).

Avoided CO_2 emission intensity with respect to the energy share shows four main clusters (Fig. 12). Systems with a temperature cut-off of 50 °C that do not use a HP result in more avoided kilograms of CO_2 per produced MWh, ranging from 265 to 302 kg/MWh. Systems with a cut-off temperature of 20 °C are limited to a range of 255–271 CO_2 kg/MWh. However, a cut-off temperature of 20 °C and the use of HP also results in larger discharge capacity leading to an increased energy share contribution and consequently to higher quantities of absolute avoided CO_2 emissions (Fig. 11) compared to a cut-off temperature of 50 °C. The energy share percentage is mostly affected by the combination of temperature cut-off and system depth. A lower cut-off temperature and a deeper system result in

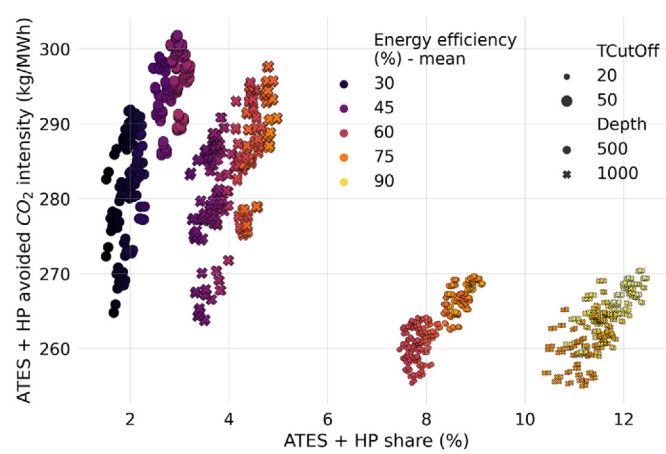

Fig. 12. Avoided CO_2 emission intensity (kg/MWh) after 15 years of operation as function of combined HT-ATES and HP energy share. It should be noted that a cut-off temperature of 50 °C implies that no HP is used in the system.

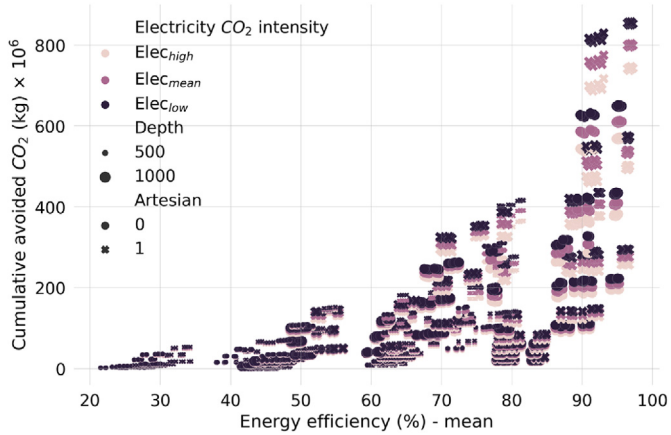

Fig. 13. Cumulative avoided CO_2 emissions over 15 years of operation as a function of energy efficiency.

higher percentage of energy share (Fig. 11). The HT-ATES energy efficiency also affects this, as systems with better efficiency achieve higher energy share.

With increasing efficiency, the cumulative avoided CO_2 emissions range increases (Fig. 13). Above an efficiency of circa 55% the range of avoided CO_2 emissions expands substantially (Fig. 13). The aquifer depth, the presence of artesian conditions and electricity grid CO_2 intensity define the final level of avoided CO_2 kg. These results are directly related to the ATES nominal capacity (see 4.1.1).

5. Discussion

Impact of regional groundwater flow on efficiency of LT-ATES systems has been analytically modelled by Ref. [61]. Their analysis shows that efficiencies below 80% are only encountered for groundwater flow velocities above 36 m/yr in small systems. Such high groundwater flow velocity for our study would only be possible via flow through conduits such as fractures and faults which we have not considered in this analysis. The regional groundwater flow levels used in our study were contextualised in the geological setting discussed (see Section 2.1) and show minor effects.

Presented simulation models assume homogeneous aquifer rock properties, which could underestimate the effect of subsurface heterogeneities. Dispersion related to aquifer heterogeneity can have significant effects on the energy efficiency of HT-ATES systems [25]. Thus, existence of strong heterogeneities can affect thermal signature extent and shape considerably, as well as associated heat recovery [62]. Therefore, characterization and subsequent inclusion of aquifer heterogeneities into simulation models should be considered in future HT-ATES studies.

Charge-store-discharge-rest profiles have a strong impact on ATES system performance. For a certain charging period a matching period of discharge is required (e.g. 1 month of charge – 1 month of discharge) to achieve a ~67% energy recovery factor, tested for periods of 1 month–4 months ([63]). The study did not use a store period between the charge and discharge periods, but did use a similar injection temperature of 90 °C, although in an aquifer with a higher initial temperature of 75 °C. Consequently, to maintain a desired energy recovery factor would entail longer periods of both HT-ATES charging and discharging, reducing the periods of storing

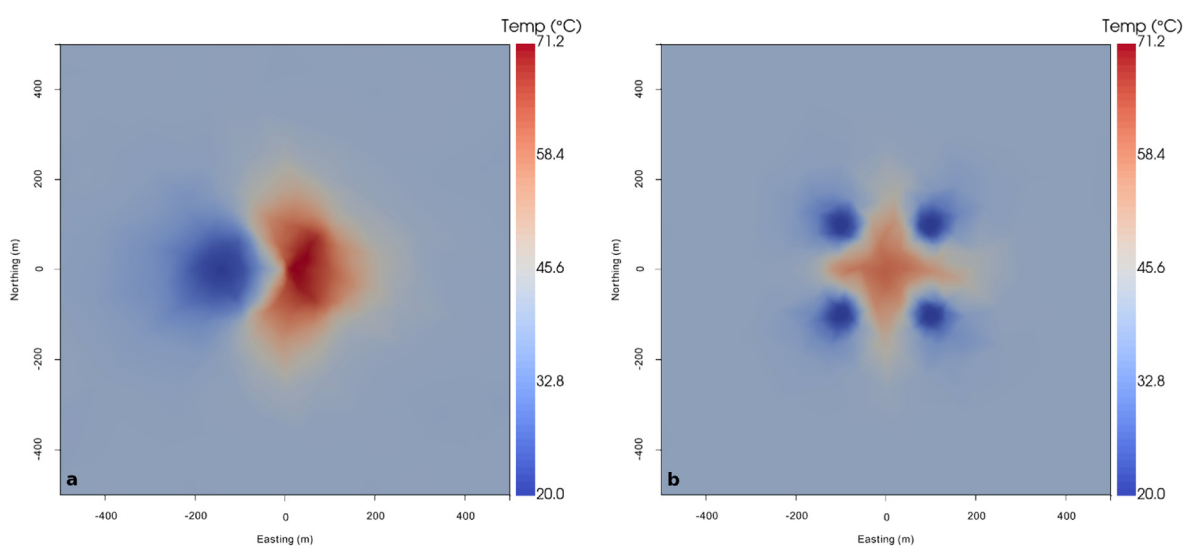

Fig. 14. HT-ATES temperature at the middle of the aquifer after 15 years of production for a doublet (a) and a 5-spot well pattern (b). Both simulations shown have an aquifer thickness 150 m, aquifer permeability 1×10^{-13}, aquifer porosity of 10%, no regional groundwater velocity, no aquifer dip, a temperature cut-off of 20 °C and an aquifer depth of 1000 m and wells spacing of 141 m.

and resting. These changes in the HT-ATES operation profile could change system efficiency and would be subject to availability of energy for charging and the demand for discharging to be utilized.

To optimise both dimensioning and energy utilization within the grid, development of a modelling framework that enables the coupling HT-ATES and DHN would be needed, as also identified in other studies [64]. This modelling framework would enable HT_ATES charging to be controlled by the DHN availability of excess heat, minimizing the amount of heat not utilized (see Fig. 9). Computational performance of such a coupled framework would be primarily hindered by the cost of modelling fluid flow and heat transfer in the subsurface. The latter may be decreased via reduction of geometric detail or accuracy in the flow-modelling approach, or with the use of proxy models [49]. With regards to system dimensioning, our study considers that sufficient energy is available for charging, and therefore the only capacity limitation is constrained by subsurface system properties. This assumption enables the HT-ATES sizing characterization and does not consider whether the required heat for charging is realistically available. Especially for systems with a large capacity (e.g. 80 MW of nominal discharge) it might be challenging to find sufficient waste heat to charge the HT-ATES system during a charging period of 4 months.

Carbon footprint reduction of a HT-ATES system can determine its long-term sustainability. HP inclusion enables reduction of the cut-off temperature to 20 °C, which leads to a nominal capacity increase and also results in higher cumulative avoided CO_2 emissions. However, this additional capacity incurs additional unrecoverable costs for installing and operating HPs, resulting in higher LCOH. While higher LCOH is undesirable, it might still enable a higher nominal capacity and energy share percentage, thus serving a higher heat demand with a baseload renewable source. This option might be preferable when design decisions are not solely based on economic criteria and quota with respect to a renewable energy share need to be honored. Examples of such quota are EU RES share of 27% for heating and cooling by 2030 [2] and 80% RES share in the DHN in Geneva [9].

LCOH exhibits an inverse relationship with nominal system capacity over the whole dataset analysed. Transmissivity is crucial here since, all else being equal, higher transmissivity enables higher nominal capacity while the CapEx are not changed, therefore lower LCOH values are reached. The analysis reveals that to keep LCOH below 200 CHF/MWh a minimum transmissivity of 2.5×10^{-12} m^3 is required. This value is five times higher than the recently presented analytical estimation of 5×10^{-13} m^3 by Ref. [34] as a minimum value of economically viable transmissivity, though that study uses 25 years of HT-ATES project. It should be noted that similar to other economic studies [65] we consider 15 years as the project duration; however, such systems could be operated for longer periods (e.g. 30 years as in Refs. [66,67]) which would reduce LCOH and thus further improve the competitiveness of HT-ATES systems.

LCOH shows the highest sensitivity to inputs of all other results presented in this study, which is similar to studies in geothermal systems that identify economic parameters as able to highlight all systems dynamics [68,69]. Therefore, the combined techno-economic assessment methodology presented in this work is preferable for initial screening and planning of HT-ATES to studies limited to either only subsurface aspects, or studies only considering DHN dynamics. Based on extensive number of parameters and their combinations considered, aquifer porosity and aquifer dip ranges show minimal impact to LCOH.

Our analysis quantifies the CO_2 emissions reduction possible from HT-ATES systems, an important aspect of their appeal and contribution to sustainability goals [70]. Limited to HT-ATES and HP operation, up to 0.8 billion kg can be avoided cumulatively over 15 years of operation with the largest systems modelled. The range of avoided CO_2 emissions per produced MWh is mostly determined by cut-off temperature and system depth. HP addition reduces the avoided CO_2 emissions per produced MWh due to additional HP operation electricity required. Nonetheless, operational CO_2 reduction is significant and can have major impacts in decarbonization the energy sector. Combined with longer lifetimes as discussed earlier, additional CO_2 reductions can be achieved. A potential Life Cycle Assessment (LCA) would better contextualize HT-ATS environmental impact and assess the full CO_2 intensity including both system construction and decommissioning, but was beyond the scope of this study.

Subsurface mechanical and chemical effects should also be addressed for HT-ATES projects, but fall outside the scope of this work. Mechanical effects are only indirectly considered in our study by using an upper flow rate limit based on the overburden pressure. Nonetheless, the impact of mechanical effects should be part of the subsurface analysis to avoid unwanted effects, especially in densely populated areas. For the Geneva HT-ATES, minor mechanical effects were identified via coupled THM modelling [71]. Additionally, geochemical analysis should be conducted to ensure adverse effects are not triggered by high temperature water injected to shallower layers. For the Geneva HT-ATES, laboratory batch experiments showed that calcite could precipitate inside the reservoir, while corrosion of wells and surface equipment could occur [71,72].

6. Conclusions

In this work we present a methodology for techno-economic and CO_2 emissions assessment of HT-ATES systems, combining demand-driven and subsurface constrained dimensioning, and contextualised in the city of Geneva, Switzerland. We develop a novel multi-criteria approach combining subsurface characterization, and energy system integration, implemented in a modelling framework “from waste to resource” which represents a unique case study for UTES solutions and in general for direct uses of geothermal energy. Subsurface characterization is based on data gathered from industry partners carrying out an ambitious geothermal exploration program and interested in exploring the potential of HT-ATES in Geneva. The results provide researchers and industry with a methodology and large dataset to assess HT-ATES efficiency for integration in energy planning studies. Moreover, our results connect HT-ATES dimensioning and efficiency to their LCOH and operational CO_2 emissions reduction which is lacking in current scientific literature.

Dimensionless DHN hourly energy demand is scaled according to HT-ATES capacity, ensuring sufficient energy for charging. HT-ATES performance is analysed using a fixed charge-discharge pattern for a period of 15 years. Thermal-hydraulic simulations are used to constrain HT-ATES capacity based on subsurface properties, using a pressure limit at 80% of lithostatic pressure. Considered parameters are hydro-geologic aquifer properties of thickness, permeability, porosity, depth, dip, artesian conditions, and regional hydraulic gradient, as well as the operational ones of well pattern and cut-off temperature. An economic model is developed to assess the Levelized Cost of Heat (LCOH) and HT-ATES CO_2 emissions are assessed for different electricity intensity

scenarios. The methodology presented opens the possibility for fully-coupled assessment of DHN and HT-ATES systems and we expect a tighter integration between the two in future research and application.

Our results show that, subject to subsurface constraints, nominal discharge capacity ranges from 0.4 MW to 81 MW, with transmissivity (product of aquifer permeability and thickness) being the major control variable. LCOH is sensitive to more input parameters but transmissivity remains dominant, followed by well pattern, cut-off temperature and aquifer depth. A minimum transmissivity of 2.5×10^{-12} m^3 is required to keep LCOH below 200 CHF/MWh and a capacity of 25 MW or higher is needed for HT-ATES to become competitive with other large-scale DHN heat sources. HP addition increases both capital and operational expenses and while system capacity increases, LCOH increases as well. Similarly, HP addition results in higher CO_2 intensity (kg CO_2/MWh) compared to systems with a cut-off temperature of 50 °C due to additional HP pumping needed. Nonetheless, systems with a 20 °C cut-off temperature result in higher nominal discharge capacity and avoid the emission of higher quantities of CO_2 in absolute values. Therefore, HP addition is only justified when a capacity increase is desired over a more economic development. Energy-to-exergy efficiency ratio is close to unity for 50 °C cut-off temperature and moves to values above ~1.3 for 20 °C cut-off temperature models.

Combined HT-ATES and HP energy share is determined by cut-off temperature and aquifer depth. With aquifer depths of 1000 m this share reaches up to ~12%, while systems at a depth of 500 m are limited to a maximum of ~5%. For comparable levels of energy share, transmissivity, artesian conditions and well pattern determine the amount of avoided CO_2 emissions in decreasing order of importance. Lastly, systems with large nominal capacity and high efficiency can lead to significant CO_2 emission reductions, in excess of 0.8 billion kg of CO_2 within a 15 years period of operation.

Credit author statement

Alexandros Daniilidis: Conceptualisation, Methodology, Software, Formal analysis, Investigation, Resources, Data curation, Writing – original draft, Writing – review & editing, Visualization. **Julian Mindel**: Methodology, Resources, Software, Formal analysis, Investigation, Data curation, Writing – original draft, Writing – review & editing, **Fleury De Oliveira Filho**: Methodology, Investigation, Resources, Writing – original draft, Writing – review & editing, **Luca Guglielmetti**: Conceptualisation, Writing – original draft, Writing – review & editing, Funding acquisition.

Funding

This work has been funded by the HEATSTORE program. HEATSTORE (170153-4401) is one of nine projects under the GEOTHERMICA – ERA NET Cofund aimed at accelerating the uptake of geothermal energy in Europe. The project is subsidized through the ERANET cofund GEOTHERMICA (Project n. 731117) by the European Commission, RVO (the Netherlands), DETEC (Switzerland), FZJ-PtJ (Germany), ADEME (France), EUDP (Denmark), Rannis (Iceland), VEA (Belgium), FRCT (Portugal), and MINECO (Spain). More information is available via http://www.heatstore.eu

Declaration of competing interest

The authors declare that they have no known competing financial interests or personal relationships that could have appeared to influence the work reported in this paper.

Acknowledgements

The authors would like to acknowledge the input and constructive discussions with Michel Meyer, Carole Nawratil de Bono and Loïc Quiquerez from Services Industriels de Genève (SIG). Moreover the authors are thankful to Andrea Moscariello for his contribution to securing funding and for his help in defining the scope of this paper.

Appendix A

Aquifer temperature after 15 years of operation is different depending on the well pattern used (Figure 14). The doublet pattern results in higher aquifer temperature by about 10 °C (Figure 14a) compared to the 5-spot well pattern (Figure 14b). However, the temperature disturbance of both well configurations has a comparable lateral extent (circa 400 × 400 m).

References

[1] Isaac M, van Vuuren DP. Modeling global residential sector energy demand for heating and air conditioning in the context of climate change. Energy Pol 2009;37:507–21. https://doi.org/10.1016/j.enpol.2008.09.051.
[2] Fleiter T, Steinbach J, Ragwitz M, Dengler J, Köhler B, Dinkel A, et al. Mapping and analyses of the current and future (2020 - 2030) heating/cooling fuel deployment. fossil/renewables; 2016. p. 1–26.
[3] Eurostat. Energy consumption in households. https://ec.europa.eu/eurostat/statistics-explained/index.php?title=Energy_consumption_in_households#Context; 2020.
[4] de Geneve Canton. Statistiques cantonales - energie 2020:1. https://www.ge.ch/statistique/graphiques/affichage.asp?filtreGraph=08_02&dom=1. [Accessed 25 February 2021].
[5] Quiquerez L. Décarboner le système énergétique à l'aide des réseaux de chaleur: état des lieux et scénarios prospectifs pour le canton de Genève. Université de Genève; 2017. https://doi.org/10.13097/archive-ouverte/unige:93380. https://archive-ouverte.unige.ch/unige:93380.
[6] Werner S. District heating and cooling in Sweden. Energy 2017;126:419–29. https://doi.org/10.1016/j.energy.2017.03.052.
[7] Lund H, Werner S, Wiltshire R, Svendsen S, Thorsen JE, Hvelplund F, et al. 4th Generation District Heating (4GDH): integrating smart thermal grids into future sustainable energy systems. Energy 2014;68:1–11. https://doi.org/10.1016/j.energy.2014.02.089.
[8] Quiquerez L, Lachal B, Monnard M, Faessler J. The role of district heating in achieving sustainable cities: comparative analysis of different heat scenarios for Geneva. Energy Proc 2017;116:78–90. https://doi.org/10.1016/j.egypro.2017.05.057.
[9] du territoire Département. Plan directeur de l'énergie 2020-2030 2020:35. https://www.ge.ch/document/plan-directeur-energie-2020-2030. [Accessed 8 January 2021].
[10] Quiquerez L, De Oliveira Filho F, Faÿ S, Hollmuller P, Meyer M. Scenarios for integration of medium-depth geothermal energy in an evolving district heating system: case study in Geneva (Switzerland). Proc. World Geotherm. Congr. 2020:2020.
[11] Arnaudo M, Dalgren J, Topel M, Laumert B. Waste heat recovery in low temperature networks versus domestic heat pumps - a techno-economic and environmental analysis. Energy 2021;219:119675. https://doi.org/10.1016/J.ENERGY.2020.119675.
[12] Arnaudo M, Topel M, Puerto P, Widl E, Laumert B. Heat demand peak shaving in urban integrated energy systems by demand side management - a techno-economic and environmental approach. Energy 2019;186:115887. https://doi.org/10.1016/J.ENERGY.2019.115887.
[13] IRENA. Renewable. Energy in district heating and cooling: a sector roadmap for REmap. Abu Dabi; 2017.
[14] Lund JW, Toth AN. Direct utilization of geothermal energy 2020 worldwide review. World Geotherm. Congr.; 2020. p. 1–39.
[15] European Commission. A European green deal. 2019. https://ec.europa.eu/info/strategy/priorities-2019-2024/european-green-deal_en.
[16] Yan J, Yang X. Thermal energy storage: an overview of papers published in Applied Energy 2009–2018. Appl Energy 2021;285:116397. https://doi.org/10.1016/j.apenergy.2020.116397.
[17] Hoekstra N, Pellegrini M, Bloemendal M, Spaak G, Andreu Gallego A, Rodriguez Comins J, et al. Increasing market opportunities for renewable energy technologies with innovations in aquifer thermal energy storage. Sci Total Environ 2020;709:136142. https://doi.org/10.1016/j.scitotenv.2019.136142.
[18] Fleuchaus P, Schüppler S, Bloemendal M, Guglielmetti L, Opel O, Blum P. Risk analysis of high-temperature aquifer thermal energy storage (HT-ATES). Renew Sustain Energy Rev 2020;133:110153. https://doi.org/10.1016/j.rser.2020.110153.
[19] Böhm H, Lindorfer J. Techno-economic assessment of seasonal heat storage in

district heating with thermochemical materials. Energy 2019;179:1246–64. https://doi.org/10.1016/J.ENERGY.2019.04.177.
[20] Guglielmetti L, Maragna C, Maurel C, Hamm V, Koorneef J, Peter O, et al. HEATSTORE: T1.3: screening of national potential for UTES. 2021.
[21] Provoost M, Albeda L, Godschalk B, Werff van der B, Schoof F. Geothermal energy use, country update for The Netherlands. The Hague, The Netherlands: Eur. Geotherm. Congr.; 2019. p. 8.
[22] Pellegrini M, Bloemendal M, Hoekstra N, Spaak G, Andreu Gallego A, Rodriguez Comins J, et al. Low carbon heating and cooling by combining various technologies with Aquifer Thermal Energy Storage. Sci Total Environ 2019;665:1–10. https://doi.org/10.1016/j.scitotenv.2019.01.135.
[23] Fleuchaus P, Godschalk B, Stober I, Blum P. Worldwide application of aquifer thermal energy storage – a review. Renew Sustain Energy Rev 2018;94:861–76. https://doi.org/10.1016/j.rser.2018.06.057.
[24] Bär K, Rühaak W, Welsch B, Schulte D, Homuth S, Sass I. Seasonal high temperature heat storage with medium deep borehole heat exchangers. Energy Proc 2015;76:351–60. https://doi.org/10.1016/j.egypro.2015.07.841. Elsevier Ltd.
[25] Zeghici RM, Oude Essink GHP, Hartog N, Sommer W. Integrated assessment of variable density-viscosity groundwater flow for a high temperature monowell aquifer thermal energy storage (HT-ATES) system in a geothermal reservoir. Geothermics 2015;55:58–68. https://doi.org/10.1016/j.geothermics.2014.12.006.
[26] Kabus F, Richlak U, Beuster H. Aquiferwärmespeicher Neubrandenburg vermittelt zwischen GuD-Kraftwerk und Fernwärmenetz. Thermische Energiespeicher der Energieversorgung; 2012.
[27] GTN.. Geothermische Nutzung des tiefen Untergrundes in Neubrandenburg - Aquiferwärmespeicher vermittelt zwischen GuD. 2016.
[28] Yang T, Liu W, Kramer GJ, Sun Q. Seasonal thermal energy storage: a techno-economic literature review. Renew Sustain Energy Rev 2021;139:110732. https://doi.org/10.1016/j.rser.2021.110732.
[29] Schüppler S, Fleuchaus P, Blum P. Techno-economic and environmental analysis of an aquifer thermal energy storage (ATES) in Germany. Geotherm Energy 2019;7:1–24. https://doi.org/10.1186/s40517-019-0127-6.
[30] Collignon M, Klemetsdal ØS, Møyner O, Alcanié M, Rinaldi AP, Nilsen H, et al. Evaluating thermal losses and storage capacity in high-temperature aquifer thermal energy storage (HT-ATES) systems with well operating limits: insights from a study-case in the Greater Geneva Basin, Switzerland. Geothermics 2020;85:101773. https://doi.org/10.1016/j.geothermics.2019.101773.
[31] Heatstore. Roadmap for flexible energy systems with underground thermal energy storage towards. 2021. p. 2050.
[32] Narula K, De Oliveira Filho F, Chambers J, Romano E, Hollmuller P, Patel MK. Assessment of techno-economic feasibility of centralised seasonal thermal energy storage for decarbonising the Swiss residential heating sector. Renew Energy 2020;161:1209–25. https://doi.org/10.1016/j.renene.2020.06.099.
[33] Liu W. The potential of high-temperature aquifer thermal energy storage (HT-ATES) to enhance the techno-economic performance of Dutch district heating systems. In: 2 Proceedings Int. Conf. Appl. Energy; 2019. p. 1–4.
[34] Birdsell DT, Adams BM, Saar MO. Minimum transmissivity and optimal well spacing and flow rate for high-temperature aquifer thermal energy storage. Appl Energy 2021;289. https://doi.org/10.1016/j.apenergy.2021.116658.
[35] Guelpa E, Verda V. Thermal energy storage in district heating and cooling systems: a review. Appl Energy 2019;252:113474. https://doi.org/10.1016/j.apenergy.2019.113474.
[36] Limberger J, Boxem T, Pluymaekers M, Bruhn D, Manzella A, Calcagno P, et al. Geothermal energy in deep aquifers: a global assessment of the resource base for direct heat utilization. Renew Sustain Energy Rev 2018;82:961–75. https://doi.org/10.1016/j.rser.2017.09.084.
[37] Kempf O, Adrian Pfiffner O. Early tertiary evolution of the North Alpine foreland basin of the Swiss Alps and adjoining areas. Basin Res 2004;16:549–67. https://doi.org/10.1111/j.1365-2117.2004.00246.x.
[38] Kuhlemann J, Kempf O. Post-eocene evolution of the North Alpine foreland basin and its response to Alpine tectonics. Sediment Geol 2002;152:45–78. https://doi.org/10.1016/S0037-0738(01)00285-8.
[39] Mazurek M, Hurford AJ, Leu W. Unravelling the multi-stage burial history of the Swiss Molasse Basin: integration of apatite fission track, vitrinite reflectance and biomarker isomerisation analysis. Basin Res 2006;18:27–50. https://doi.org/10.1111/j.1365-2117.2006.00286.x.
[40] Brentini M. Impact d'une donnée géologique hétérogène dans la gestion des géo-ressources: analyse intégrée et valorisation de la stratigraphie à travers le bassin genevois (Suisse, France). University of Geneva; 2018. https://doi.org/10.13097/archive-ouverte/unige:103409.
[41] Jenny J, Burri JP, Muralt R, Pugin A, Schegg R, Ungemach P, et al. Le forage géothermique de Thônex (Canton de Genève): aspects stratigraphiques, tectoniques, diagénétiques, géophysiques et hydrogéologiques. Eclogae Geol Helv 1995;88:365–96.
[42] Moscariello A. Exploring for geo-energy resources in the Geneva Basin (Western Switzerland): opportunities and challenges. Swiss Bull Für Angew Geol 2019;24:105–24.
[43] Rusillon E. Characterisation and rock typing of deep geothermal reservoirs in the Greater Geneva Basin (Switzerland & France). 2017. https://doi.org/10.13097/archive-ouverte/unige:105286. University of Geneva.
[44] Clerc N. A revised structural framework for the Geneva Basin and the neighboring France region as revealed from 2D seismic data: implications for geothermal exploration. Swiss Bull Für Angew Geol 2020;25:109–31.
[45] SITG. Le territoire genevois à la carte 2021. https://ge.ch/sitg/. [Accessed 8 January 2021].
[46] Østergaard PA. Reviewing EnergyPLAN simulations and performance indicator applications in EnergyPLAN simulations. Appl Energy 2015;154:921–33. https://doi.org/10.1016/j.apenergy.2015.05.086.
[47] Reinholdt L, Kristófersson J, Zühlsdorf B, Elmegaard B, Jensen J, Ommen T, et al. Heat pump COP, part 1: generalized method for screening of system integration potentials. Refrig. Sci. Technol. 2018;2018:1207–13. https://doi.org/10.18462/iir.gl.2018.1380. June, International Institute of Refrigeration.
[48] Jensen JK, Ommen T, Reinholdt L, Markussen WB, Elmegaard B. Heat pump COP, part 2: generalized COP estimation of heat pump processes. Refrig. Sci. Technol. 2018;2018:1255–64. https://doi.org/10.18462/iir.gl.2018.1386. June, International Institute of Refrigeration.
[49] Allaerts K, de Oliveira Filho F, Hollmuller P, Guglielmetti L, Quiquerez L, Maranga C, et al. UTES and its integration in the heating system -Defining optimal design and operational strategies for the demonstration cases. 2021.
[50] Mindel JE, Alt-Epping P, Landes AA Les, Beernink S, Birdsell DT, Bloemendal M, et al. Benchmark study of simulators for thermo-hydraulic modelling of low enthalpy geothermal processes. Geothermics 2021;96:102130. https://doi.org/10.1016/j.geothermics.2021.102130.
[51] Haar L, Gallagher JS, Kell GS. NBS/NRC steam tables: thermodynamic and transport properties and computer programs for vapor and liquid states of water in SI units. Washington, DC: Hemisphere; 1964. 1984.
[52] Huber ML, Perkins RA, Laesecke A, Friend DG, Sengers JV, Assael MJ, et al. New international formulation for the viscosity of H2 O. J Phys Chem Ref Data 2009;38:101–25. https://doi.org/10.1063/1.3088050.
[53] Mindel JE, Driesner T. HEATSTORE: preliminary design of a high temperature aquifer thermal energy storage (HT-ATES) system in Geneva based on TH simulations. Proc. World Geotherm. Congr. 2020:1–12. https://doi.org/10.3929/ethz-b-000444531. 2020+1.
[54] Dincer I, Rosen M. Thermal energy storage systems and applications. 2011.
[55] TNO. ThermoGIS v2.0 - economic model. 2018. ThermoGIS v20, https://www.thermogis.nl/en/economic-model. [Accessed 2 July 2019].
[56] Meyer M. Concepts d'utilisation énergétique du puits GEo-01. 2019.
[57] de Geneve Canton. Tarification du chauffage à distance par l'incinération des ordures ménagères. 2018.
[58] Arpagaus C, Bertsch S. Industrial heat pumps in Switzerland application potentials and case studies. Bern; 2020.
[59] KBOB;, Eco-bau;, IPB. Ökobilanzdaten im Baubereich 2009/1. 2016. :2016.
[60] Zuberi MJ., Chambers J, Patel MK. Techno-economic comparison of technology options for deep decarbonization and electrification of residential heating. Under Rev n.d.
[61] Bloemendal M, Hartog N. Analysis of the impact of storage conditions on the thermal recovery efficiency of low-temperature ATES systems. Geothermics 2018;71:306–19. https://doi.org/10.1016/j.geothermics.2017.10.009.
[62] Sommer W, Valstar J, Van Gaans P, Grotenhuis T, Rijnaarts H. The impact of aquifer heterogeneity on the performance of aquifer thermal energy storage. Water Resour Res 2013;49:8128–38. https://doi.org/10.1002/2013WR013677.
[63] Major M, Poulsen SE, Balling N. A numerical investigation of combined heat storage and extraction in deep geothermal reservoirs. Geotherm Energy 2018;6:1. https://doi.org/10.1186/s40517-018-0089-0.
[64] Liu Z, Zhao Y, Wang X. Long-term economic planning of combined cooling heating and power systems considering energy storage and demand response. Appl Energy 2020;279:115819. https://doi.org/10.1016/j.apenergy.2020.115819.
[65] Wesselink M, Liu W, Koornneef J, van den Broek M. Conceptual market potential framework of high temperature aquifer thermal energy storage - a case study in The Netherlands. Energy 2018;147:477–89. https://doi.org/10.1016/j.energy.2018.01.072.
[66] Sommer W, Valstar J, Leusbrock I, Grotenhuis T, Rijnaarts H. Optimization and spatial pattern of large-scale aquifer thermal energy storage. Appl Energy 2015;137:322–37. https://doi.org/10.1016/j.apenergy.2014.10.019.
[67] Bloemendal M, Olsthoorn T, Boons F. How to achieve optimal and sustainable use of the subsurface for Aquifer Thermal Energy Storage. Energy Pol 2014;66:104–14. https://doi.org/10.1016/j.enpol.2013.11.034.
[68] Daniilidis A, Alpsoy B, Herber R. Impact of technical and economic uncertainties on the economic performance of a deep geothermal heat system. Renew Energy 2017;114:805–16. https://doi.org/10.1016/j.renene.2017.07.090.
[69] Daniilidis A, Khait M, Saeid S, Bruhn DF, Voskov D. A high performance framework for the optimization of geothermal systems, comparing energy production and economic output. Proc. World Geotherm. Congr. 2020:1–10. Reykjavik, Iceland: 2020.
[70] Lu H, Tian P, Guan Y, Yu S. Integrated suitability, vulnerability and sustainability indicators for assessing the global potential of aquifer thermal energy storage. Appl Energy 2019;239:747–56. https://doi.org/10.1016/j.apenergy.2019.01.144.
[71] Guglielmetti L, Houlié N, Nawtratil del Bono C, Martin F, Coudroit J. Heatstore - monitoring results for the Geneva HT-ATES case-study. 2021.
[72] Guglielmetti L, Bloemendal M, Hahn F, Mortensen MH, Koornneef J, Alt-Epping P, et al. Heatstore - environmental effects of UTES technologies in Europe. 2021.